Jurnal Teknik Informatika (JUTIF)
P-ISSN: 2723-3863
E-ISSN: 2723-3871
Vol. 7, No. 2, April 2026, Page. 1040-1055
https://jutif.if.unsoed.ac.id
DOI: https://doi.org/10.52436/1.jutif.2026.7.2.5617

Cloud Computing-Based U-Net Integration for Post-Landslide Satellite Image Segmentation

Swelandiah Endah Pratiwi*[1], Paranita Asnur[2], Fitrianingsih[3], Remi Senjaya[4], Muhammad Sahal Nurdin[5]

[1]Computer Engineering Study Program, Directorate of Information Technology Diploma, Gunadarma University, Depok, Indonesia
[2]Agrotechnology Study Program, Faculty of Agricultural Industrial Technology, Gunadarma University, Depok, Indonesia
[3]Diploma Program in Informatics Management, Universitas Gunadarma, Jakarta, Indonesia
[4,5]Information Systems Study Program, Faculty of Computer Science, Gunadarma University, Depok, Indonesia

Email: [1]swelandiah@staff.gunadarma.ac.id

Received: Jan 6, 2026; Revised: Feb 20, 2026; Accepted: Feb 22, 2026; Published: Apr 15, 2026

Abstract

Landslides are geological disasters that cause severe impacts on human life, infrastructure, and ecosystems, highlighting the need for post-disaster mapping methods that are fast, accurate, and scalable. This study aims to develop a post-landslide satellite image segmentation framework based on U-Net integrated with cloud computing to support large-scale and operational disaster mapping. While U-Net has been widely applied for landslide analysis, most existing studies focus on local-scale assessments or susceptibility mapping and lack integration with cloud-based pipelines and multi-source data for post-disaster operations. The novelty of this research lies not in modifying the U-Net architecture, but in integrating multi-source geospatial data, system workflow, and scalable cloud deployment. The proposed framework utilises a global multi-source dataset consisting of RGB imagery, Normalized Difference Vegetation Index (NDVI), slope, and elevation to enhance robustness and generalisation across diverse geomorphological conditions. Experimental results show stable model convergence with a final loss of 0.0357, an F1-score exceeding 0.75, and an AUC-PR of 0.8391. Evaluation on the testing dataset achieves a precision of 0.7692, recall of 0.7519, F1-score of 0.7604, and Intersection over Union of 0.6135. Qualitative analysis demonstrates strong spatial agreement between predicted segmentation and ground truth, with minor deviations mainly along complex slope boundaries. From an Informatics perspective, this study contributes by operationalizing deep learning through cloud computing to enable scalable computation, parallel processing, and system-level deployment, while providing object-level estimates of landslide events and affected areas to support disaster response and risk mitigation.

Keywords: *Big data analytics, Disaster mitigation, Multispectral imagery, Semantic segmentation, Spatial generalization.*

1. INTRODUCTION

Landslides represent one of the most destructive geological hazards, causing extensive losses to human life, infrastructure, and ecosystems. The Data Unified Global Landslide Database documents 37,946 landslide events across 161 countries between 1903 and 2020, resulting in 185,753 fatalities, underscoring the global severity of this disaster [1]. Asia and the Americas record the highest frequency of landslide occurrences, driven by the combined influence of geological conditions, extreme rainfall, and rapid land-use change [2]. The spatial extent and complex triggering mechanisms of landslides necessitate post-disaster monitoring systems that operate rapidly, accurately, and at large scale to support effective and sustainable mitigation strategies [3], [4].

Remote sensing and spatial analysis have become central to post-landslide mapping due to their ability to provide timely and synoptic observations [5]. Sentinel-2 imagery effectively captures changes

Vol. 7, No. 2, April 2026, Page. 1040-1055
https://jutif.if.unsoed.ac.id
DOI: https://doi.org/10.52436/1.jutif.2026.7.2.5617

in vegetation cover and slope morphology associated with landslide events [6], [7]. The fusion of optical and radar data further improves detection robustness under variable surface and atmospheric conditions [8], while the integration of DEM or LiDAR data and spectral indices enriches geomorphological characterization [9]. However, extracting accurate landslide boundaries from these heterogeneous data sources remains challenging when using conventional image analysis techniques.

Recent advances in deep learning, particularly convolutional neural network based image segmentation, have significantly improved object delineation in complex scenes. Among these approaches, the U-Net architecture has emerged as a dominant model due to its encoder–decoder structure with skip connections that preserve spatial resolution and enable precise boundary reconstruction [10]. Beyond landslide applications, U-Net and its variants demonstrate strong performance across multiple domains, confirming their robustness and generalizability. In medical imaging, U-Net-based models successfully perform multi-class brain tumor segmentation and classification from MRI data, even under limited annotated samples [11], [12]. In agricultural contexts, enhanced U-Net CNN architectures effectively segment and classify rice leaf diseases under real field conditions in Indonesian rice fields [13]. These studies show that U-Net can handle heterogeneous image characteristics, class imbalance, and complex object boundarie conditions that closely resemble post-landslide satellite imagery.

Methodologically, landslide mapping studies have evolved from classical CNN and feature-based models, which rely on handcrafted features and patch-level classification, toward standard U-Net architectures that enable end-to-end semantic segmentation with improved boundary accuracy [14]-[16]. More recent works introduce U-Net variants, such as Attention U-Net and U-Net++, to enhance multi-scale representation and focus on salient landslide features [17], [18].

Nevertheless, a substantial portion of existing studies primarily targets landslide susceptibility mapping or pre-event analysis, while fewer studies emphasize post-disaster segmentation aimed at rapid damage assessment and operational response [19], [20].

Despite these advances, several critical gaps remain evident: (1) most studies rely on local or region-specific datasets, limiting model generalization; (2) multi-source data integration is often partial or absent; (3) cloud based deploymentis rarely implemented as a core research component; and (4) post-segmentation analysis is typically restricted to pixel-level accuracy metrics without object-level interpretation, such as estimating the number of landslide events or affected areas [21], [22]. Addressing these gaps, this research positions its novelty at the integration of U-Net-based post-landslide segmentation, multi-source satellite data, and cloud computing infrastructure. Unlike prior studies that focus on model performance alone, this work emphasizes scalability, operational deployment, and object-level analysis to support real-world disaster management.

Accordingly, the objective of this study is to develop a cloud computing–based U-Net segmentation system that improves accuracy, scalability, and operational readiness for post-landslide satellite image analysis, thereby providing reliable and actionable information to support disaster response and risk mitigation across diverse regions.

Unlike studies that focus on architectural modification of deep learning models, the novelty of this research lies in system-level integration. Specifically, this work contributes through: (1) multi-source geospatial data fusion combining spectral and terrain-derived features, (2) cloud-based scalable processing pipeline enabling operational deployment, and (3) object-level post-processing that transforms pixel-level segmentation into structured disaster indicators such as landslide event counts and affected area estimation.

Vol. 7, No. 2, April 2026, Page. 1040-1055
https://jutif.if.unsoed.ac.id
DOI: https://doi.org/10.52436/1.jutif.2026.7.2.5617

2. METHOD

This study utilises a deep learning approach based on the U-Net architecture for segmenting satellite images of landslides after disasters. The research process includes six stages (Figure 1): data collection, pre-processing, U-Net architecture design, model training, evaluation–testing, and web-based system implementation. Each stage is equipped with a feedback mechanism to iteratively improve the quality of the results.

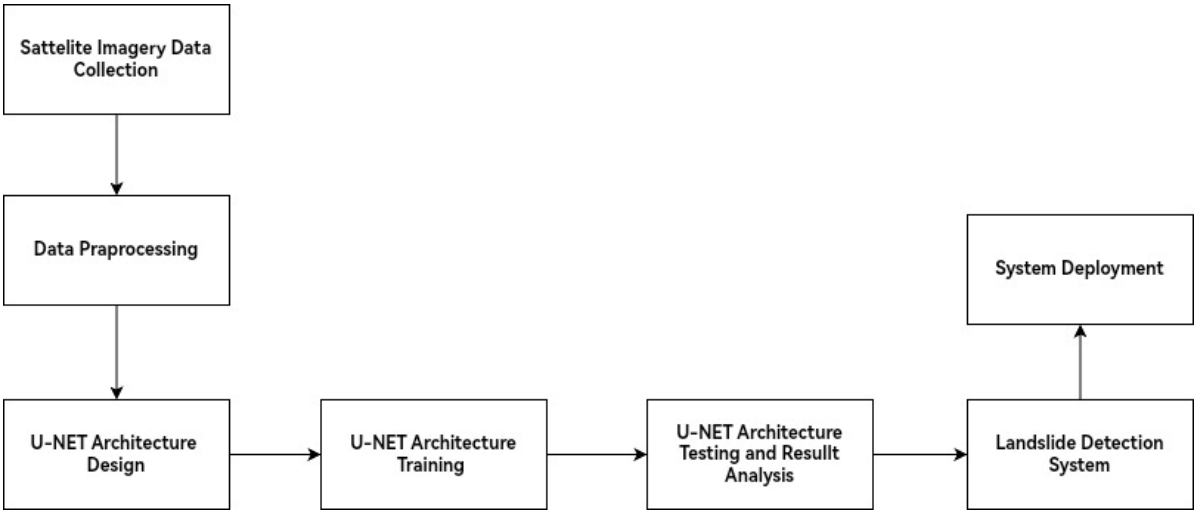

Figure 1. Research Flowchart

It is important to note that this study does not propose a new neural network architecture. Instead, it focuses on integrating a well-established U-Net segmentation backbone into an operational pipeline that combines multi-source geospatial data and cloud-based computing infrastructure for real-world disaster monitoring applications. Therefore, the primary contribution of this work lies in enhancing system scalability, improving robustness through multi-source feature integration, and enabling decision-support capability for operational disaster response rather than introducing architectural modifications at the model level.

2.1. Data Collection

The dataset used in this study is derived from the Landslide4Sense benchmark dataset, consisting of 3,799 Sentinel-2 satellite images with a spatial resolution of 10 m/pixel, accompanied by manually annotated ground truth segmentation masks. The dataset includes multispectral channels (B1–B12), geomorphological information such as slope and Digital Elevation Model (DEM) derived from ALOS PALSAR, as well as Normalized Difference Vegetation Index (NDVI) computed from red and near-infrared bands. The Landslide4Sense dataset represents a global multi-regional collection of landslide events captured across diverse geomorphological and climatic conditions, including mountainous tropical environments, temperate regions, and areas with varying vegetation density and rainfall intensity. This diversity enables the model to learn generalized spatial characteristics of landslide morphology across different environmental contexts, thereby reducing region-specific bias and improving model generalization capability. To ensure robust model development and unbiased evaluation, the dataset is partitioned into 70% training data, 20% validation data, and 10% testing data, allowing the model to learn data variability while maintaining independent performance assessment. Furthermore, the global and multi-source nature of the dataset supports the development of scalable deep learning models suitable for large-scale operational disaster monitoring applications.

Jurnal Teknik Informatika (JUTIF)
P-ISSN: 2723-3863
E-ISSN: 2723-3871
Vol. 7, No. 2, April 2026, Page. 1040-1055
https://jutif.if.unsoed.ac.id
DOI: https://doi.org/10.52436/1.jutif.2026.7.2.5617

2.2. Data Preprocessing

Preprocessing encompasses the imputation of missing values (NaN) through spatial interpolation, the construction of feature channels (RGB, NDVI, slope, elevation), and normalisation to the range [0,1]. This technique seeks to enhance spectral-spatial information (Figure 2) while ensuring data consistency. The multi-channel input is subsequently processed by the U-Net architecture, which is characterised by a symmetrical encoder-decoder framework and skip connections that maintain high-resolution information at the margins of the landslide region. Figure 3 illustrates a comparison of the images prior to and subsequent to normalisation.

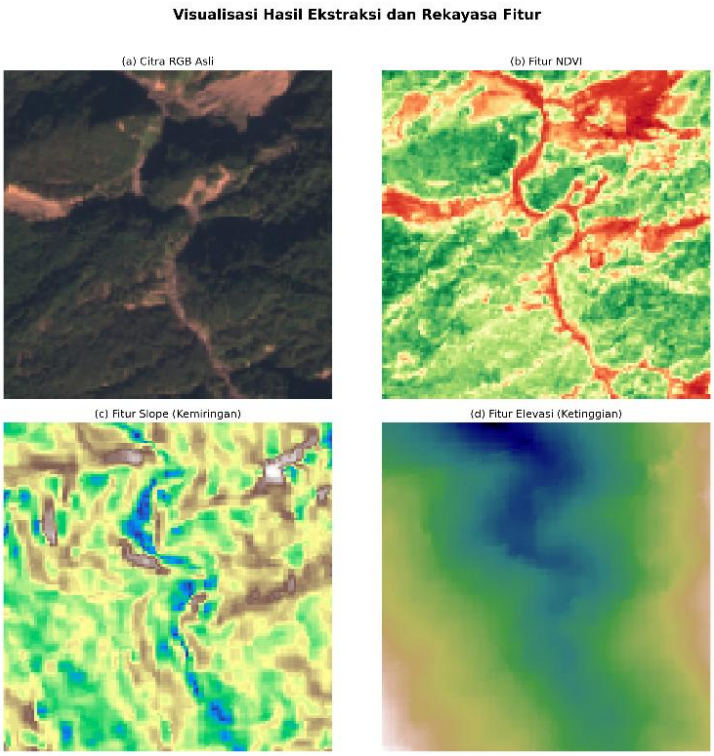

Figure 2. Visualization of satellite image feature extraction results, (a) Original RGB image, (b) NDVI, (c) Slope, and (d) Elevation.

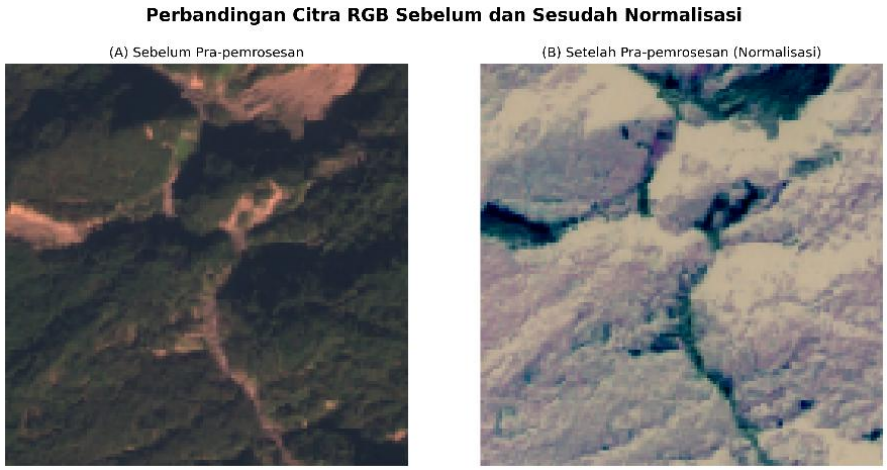

Figure 3. Image (a) RGB image before pre-processing and Image (b) RGB image after pre-processing (Normalization).

Vol. 7, No. 2, April 2026, Page. 1040-1055
https://jutif.if.unsoed.ac.id
DOI: https://doi.org/10.52436/1.jutif.2026.7.2.5617

2.3. U-Net Model Architecture

The U-Net architecture (Figure 4) used has a symmetrical encoder-decoder structure. The encoder part extracts image features through layered convolutional operations, while the decoder part performs an upsampling process to reconstruct the segmentation map. Skip connections linking the encoder and decoder allow high-resolution information to be preserved, enabling the model to generate more precise segmentations, especially in complex landslide boundary areas.

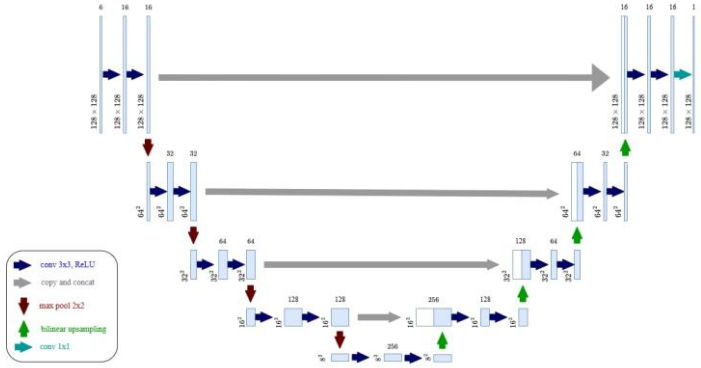

Figure 4. U-Net architecture design for landslide semantic segmentation

2.4. Model Training, Evaluation, and Testing Training

Model training was conducted using the Adam optimization algorithm with a learning rate of 0.001, batch size of 16, and 50 training epochs, which is widely adopted in deep learning optimization due to its adaptive learning capability and fast convergence performance [23]. To address class imbalance commonly observed in landslide segmentation tasks, a combined Binary Cross Entropy and Dice Loss function was employed to optimize both pixel-wise classification accuracy and spatial overlap performance [24], [25]. The model performance was quantitatively evaluated using Precision, Recall, F1-score, Accuracy, Intersection over Union (IoU), and Area Under the Precision–Recall Curve (AUC-PR), which are standard evaluation metrics for semantic segmentation and imbalanced classification problems [10], [14]. In addition, qualitative evaluation was performed by visually comparing predicted segmentation outputs with ground truth masks, as illustrated in Figure 5.

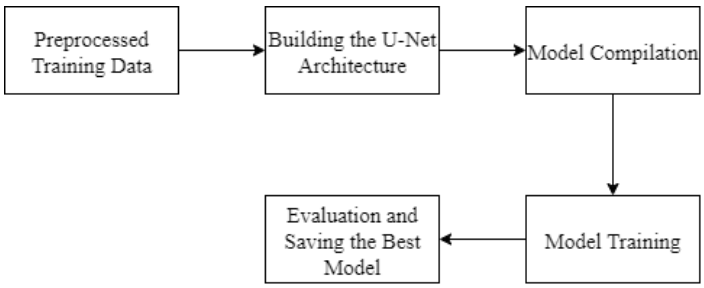

Figure 5. Learning Process Flowchart

This study utilizes multi-source input data consisting of RGB imagery, Normalized Difference Vegetation Index (NDVI), slope, and elevation features. While RGB-only inputs are widely used in semantic segmentation applications, they are often insufficient for landslide detection due to spectral similarity between exposed soil surfaces and surrounding terrain [26]. The integration of multi-source data provides complementary information, where spectral indices enhance vegetation disturbance detection and terrain-derived features improve geomorphological boundary representation [9]. Although a direct ablation comparison between RGB-only and multi-source configurations was not conducted in

Vol. 7, No. 2, April 2026, Page. 1040-1055
https://jutif.if.unsoed.ac.id
DOI: https://doi.org/10.52436/1.jutif.2026.7.2.5617

this study, previous studies have consistently demonstrated that multi-source data fusion improves segmentation robustness and spatial generalization in remote sensing applications [22]. Therefore, the performance improvements observed in this work are interpreted within the context of established literature supporting the effectiveness of multi-source geospatial data integration.

To ensure methodological transparency and reproducibility, this study formally defines the optimization objective and evaluation metrics, employing a composite Binary Cross Entropy–Dice Loss for training and standard semantic segmentation metrics to comprehensively evaluate model performance.

1. Binary Cross Entropy Loss

$$BCE = -\frac{1}{N}\sum_{i=1}^{N}[y_i * \log(\hat{y}_i) + (1 - y_i) * \log(1 - \hat{y}_i)\ ] \quad (1)$$

Where N denotes the total number of samples used during training, y_i corresponds to the true binary label of the i-th sample, and $\hat{y}_i$ indicates the predicted probability generated by the model for the i-th sample to belong to the positive class.

2. Dice Loss

$$L_{dice} = 1 - \frac{1}{C}\sum_{C=0}^{C-1}\frac{2\sum_{n=1}^{N} t_n^C y_n^C}{\sum_{n=1}^{N}(t_n^C + y_n^C)} \quad (2)$$

Dice Loss, computed from the class-averaged soft Dice coefficient using probabilistic outputs, directly optimizes spatial overlap to address class imbalance and improve segmentation performance, particularly when target regions occupy small spatial areas. To ensure objective and comprehensive performance evaluation, this study employs multiple quantitative metrics formally defined mathematically to assess classification accuracy, detection completeness, and spatial agreement in imbalanced semantic segmentation tasks such as landslide detection.

3. Precision

Precision measures the proportion of correctly predicted landslide pixels among all pixels predicted as landslide by the model.

$$Precision = \frac{True\ Positif}{True\ Positif + False\ Positif} \quad (3)$$

4. Recall

Recall measures the proportion of actual landslide pixels that are successfully detected by the model.

$$Recall = \frac{True\ Positif}{True\ Positif + False\ Negatif} \quad (4)$$

5. F1-Score

The F1-score provides a balanced evaluation between precision and recall, especially when dealing with imbalanced datasets.

$$F1 - Score = 2\ X\ \frac{Precision\ x\ Recall}{Precision + Recall} \quad (5)$$

6. Accuracy

Accuracy reflects the overall classification correctness of the model across both landslide and non-landslide classes.

Vol. 7, No. 2, April 2026, Page. 1040-1055
https://jutif.if.unsoed.ac.id
DOI: https://doi.org/10.52436/1.jutif.2026.7.2.5617

$$Accuracy = \frac{TP+TN}{TP+TN+FP+FN} \quad (6)$$

7. Intersection over Union (IoU)

IoU measures the spatial overlap between predicted segmentation regions and ground truth segmentation regions.

$$IoU = \frac{TP}{TP+FP+FN} \quad (7)$$

2.5. System Implementation

The best model was integrated into a web-based application using Flask and deployed on Google Cloud, allowing users to upload satellite images to automatically obtain landslide segmentation results. The proposed system is organized into five main layers to ensure scalable processing, modular system integration, and efficient data flow from raw satellite data acquisition to final decision-support output (Figure 6).

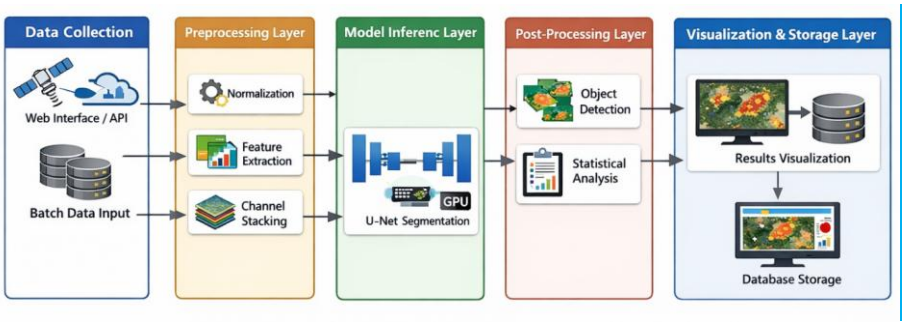

Figure 6. illustrates the cloud-based operational architecture designed to support multi-source landslide segmentation and object-level post-processing

The system consists of four layers: data collection from multi-source satellite inputs, preprocessing with normalization and feature integration (RGB, vegetation indices, terrain features), scalable cloud-based U-Net inference for semantic segmentation, and post-processing using connected component analysis to detect landslide objects and estimate affected areas. The visualization and storage layer presents segmentation results and statistical summaries through web-based dashboards while storing processed outputs in cloud databases, enabling end-to-end operational deployment for landslide monitoring that reports detection status and estimated affected areas (Figure 7).

Vol. 7, No. 2, April 2026, Page. 1040-1055
https://jutif.if.unsoed.ac.id
DOI: https://doi.org/10.52436/1.jutif.2026.7.2.5617

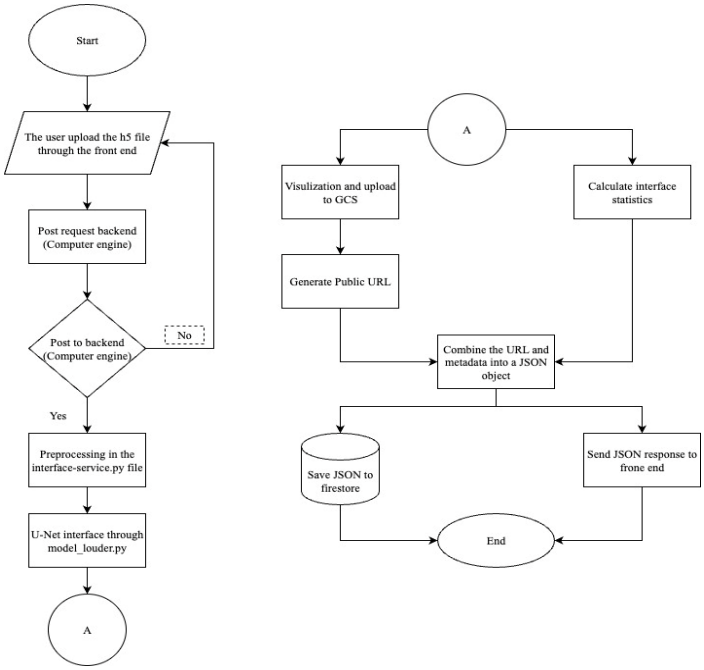

Figure 7. Backend Data Flowchart

3. RESULT

3.1. Training Model

The training and validation curves indicate stable and consistent learning behavior throughout the optimization process. The loss decreases progressively and converges smoothly, while precision, recall, F1-score, IoU, and accuracy show steady improvement before reaching stable plateaus. As illustrated in Figure 8(a–f), both training and validation losses decline sharply in the early epochs and gradually stabilize with a minimal gap, suggesting good generalization without evident overfitting. Precision and recall increase consistently across epochs, indicating improved identification of landslide pixels while maintaining balanced detection capability. This relationship is reflected in the stabilization of the F1-score after approximately 20 epochs, confirming balanced classification performance. IoU values demonstrate gradual improvement and strong spatial agreement between predicted masks and ground truth labels, while accuracy remains consistently high with closely aligned training and validation trends. Overall, the convergence patterns confirm that the U-Net architecture effectively learns discriminative spatial features for landslide segmentation and maintains stable predictive performance across evaluation metrics.

Jurnal Teknik Informatika (JUTIF)
P-ISSN: 2723-3863
E-ISSN: 2723-3871
Vol. 7, No. 2, April 2026, Page. 1040-1055
https://jutif.if.unsoed.ac.id
DOI: https://doi.org/10.52436/1.jutif.2026.7.2.5617

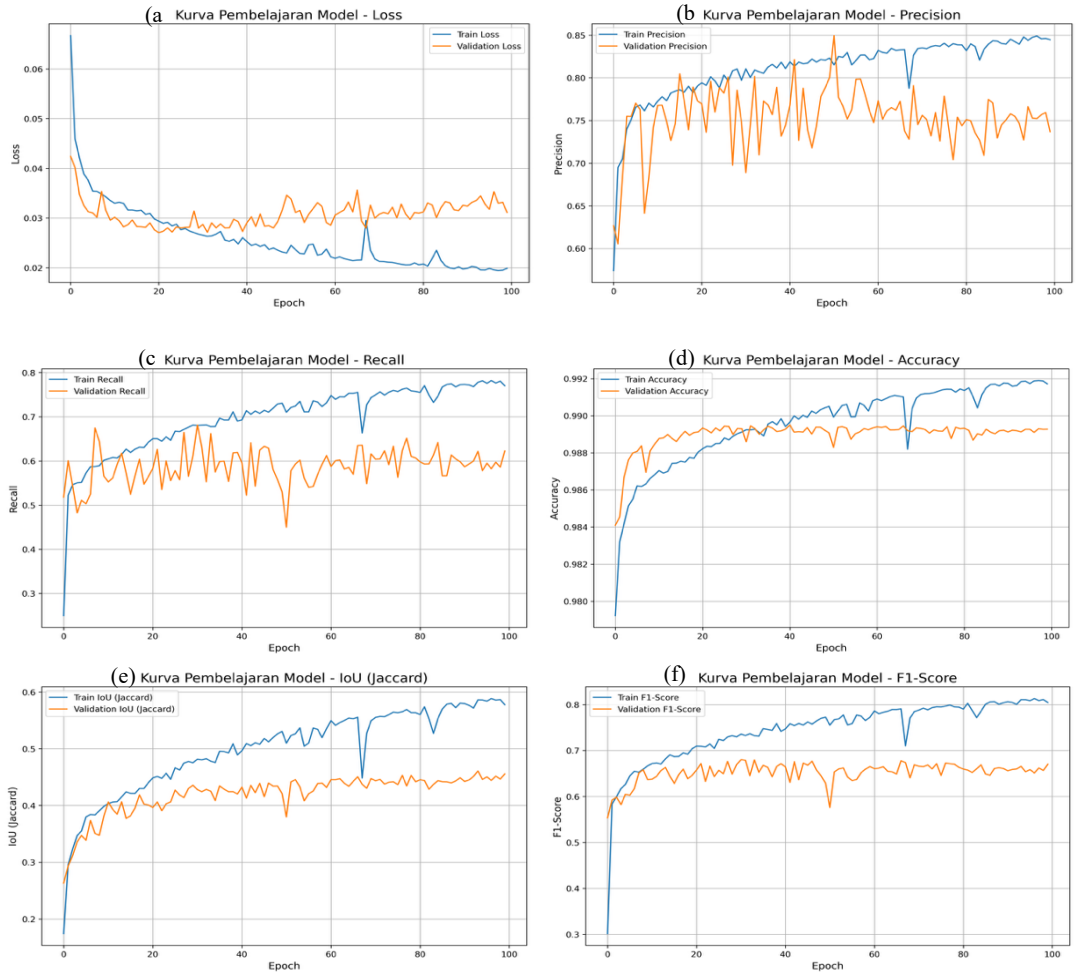

Figure 8. Training and validation performance of the U-Net model, including (a) loss curve, (b) precision curve, (c) recall curve, (d) F1-score curve, (e) Intersection over Union (IoU) curve, and (f) accuracy curve

Quantitative evaluation on the validation dataset yields 178,100 true positives, 12,132,830 true negatives, 73,347 false positives, and 67,563 false negatives, as presented in the confusion matrix (Figure 9). Visual comparisons between predicted masks and reference labels (Figure 10) show strong spatial correspondence, with minor discrepancies primarily along complex slope boundaries. Consistent prediction behavior across multiple validation samples is further illustrated in Figure 11. The integration of multi-source features RGB, NDVI, slope, and elevation (Figure 12) enhances spatial representation, contributing to IoU values exceeding 0.60 and stable AUC-PR performance on validation data.

Jurnal Teknik Informatika (JUTIF)
P-ISSN: 2723-3863
E-ISSN: 2723-3871
Vol. 7, No. 2, April 2026, Page. 1040-1055
https://jutif.if.unsoed.ac.id
DOI: https://doi.org/10.52436/1.jutif.2026.7.2.5617

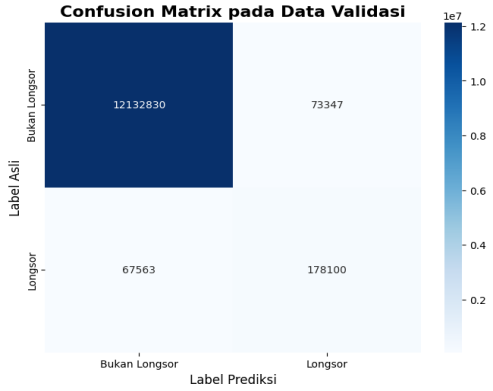

Figure 9. Confusion matrix on the validation dataset at an optimal threshold of 0.3519, showing true positive, true negative, false positive, and false negative distributions

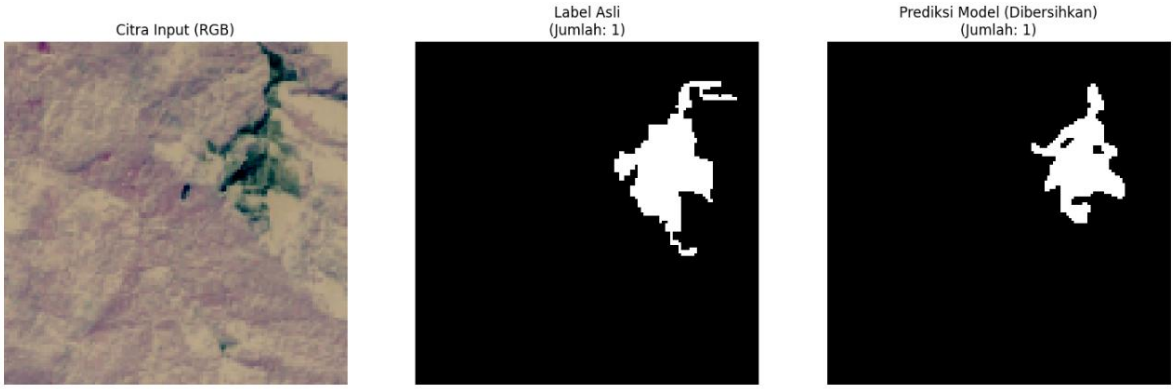

Figure 10. Example of model segmentation results on the validation dataset showing comparison between predicted masks and ground truth

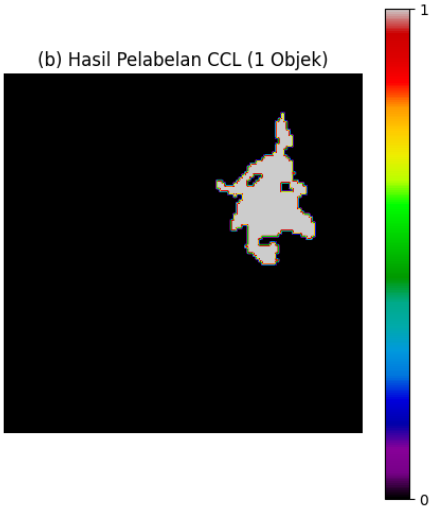

Figure 11. Consistency of segmentation and labeling results across multiple validation samples

Jurnal Teknik Informatika (JUTIF)
P-ISSN: 2723-3863
E-ISSN: 2723-3871
Vol. 7, No. 2, April 2026, Page. 1040-1055
https://jutif.if.unsoed.ac.id
DOI: https://doi.org/10.52436/1.jutif.2026.7.2.5617

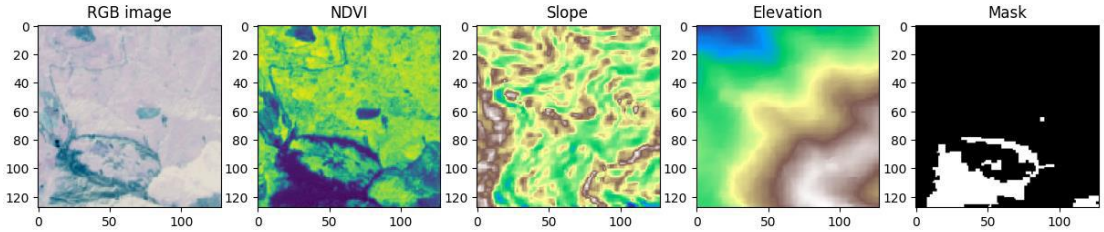

Figure 12. Multi-source input features consisting of RGB, NDVI, slope, elevation, and corresponding mask images for a representative training data sample.

3.2. Performance of the U-Net

The U-Net model demonstrates reliable performance on the Landslide4Sense testing dataset. At an optimal decision threshold of 0.3519, the model achieves a precision of 0.7692, recall of 0.7519, F1-score of 0.7604, IoU of 0.6135, accuracy of 0.9876, and AUC-PR of 0.8391, as illustrated in Figure 13. The combination of F1-score values above 0.75 and IoU values above 0.60 indicates balanced classification performance and strong spatial agreement between predicted and reference segmentation masks.

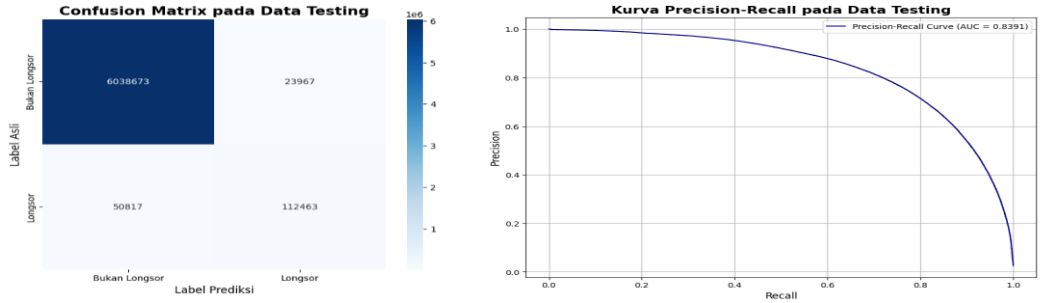

Figure 13. (a) Confusion Matrix on the testing dataset with an optimal threshold of 0.3519; (b) Precision-Recall curve on the testing data

The confusion matrix and precision–recall curve presented in Figure 13(a–b) show a stable trade-off between precision and recall across different probability thresholds. False positive detections are mainly associated with terrain regions exhibiting spectral and textural similarities to landslide areas, while false negatives are predominantly observed along fragmented boundaries and partially vegetated landslides.

Qualitative evaluation on the testing dataset (Figure 14) further confirms that the predicted segmentation maps closely follow the spatial patterns of the ground truth masks. Most landslide-affected areas are successfully identified, with remaining inaccuracies primarily occurring in complex slope transition zones.

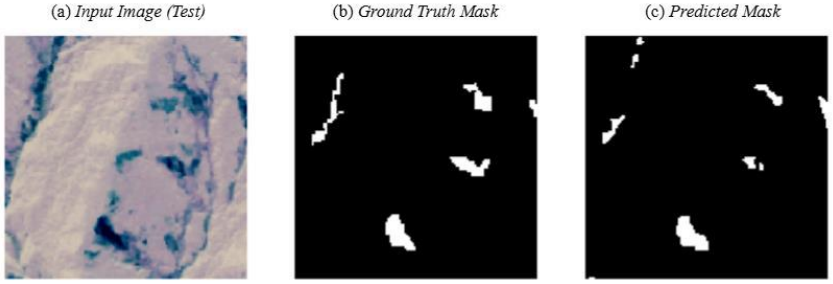

Figure 14. Qualitative segmentation results on the testing dataset: (a) input satellite image, (b) ground truth mask, and (c) predicted mask

Vol. 7, No. 2, April 2026, Page. 1040-1055
https://jutif.if.unsoed.ac.id
DOI: https://doi.org/10.52436/1.jutif.2026.7.2.5617

Post-processing using Connected Component Labeling (CCL) is applied to the segmentation outputs to reduce isolated noise and separate individual landslide objects, enabling clearer object delineation and more consistent spatial representation in the final results.

3.3. Analysis Results

Predictions on unlabeled test data (Table 1) demonstrate that the proposed U-Net framework is capable of detecting landslide events with varying numbers and spatial extents across different images. The number of detected landslide objects per image ranges from 1 to 11, with estimated affected areas spanning from several thousand to over 300,000 m². These variations indicate that the model is able to capture landslide occurrences across multiple spatial scales.

Table 1. Prediction Results for Unlabeled Test Data and Analysis of Landslide Segmentation Results

Input Image	*Predicted Mask*	Detection Status	Number of Objects Area	Objects Area Estimation Details (m²)	Total Estimated Area (m²)
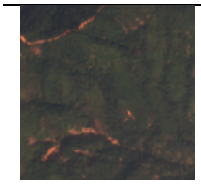		Detected	5	8700, 2500, 3300, 6000, 800	21300
		Detected	1	3000	3000
		Detected	6	21300, 13200, 9100, 3300, 8700, 5900	61500
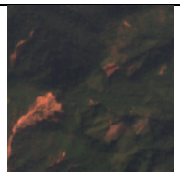		Detected	5	1200, 3400, 7000, 62600, 10700	84900
		Detected	5	11000, 14900, 5100, 3300, 13800	48100
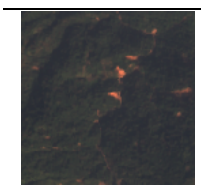	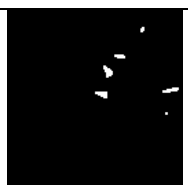	Detected	6	1000, 2100, 3700, 3100, 3300, 400	13600

Vol. 7, No. 2, April 2026, Page. 1040-1055
https://jutif.if.unsoed.ac.id
DOI: https://doi.org/10.52436/1.jutif.2026.7.2.5617

Input Image	*Predicted Mask*	Detection Status	Number of Objects Area	Objects Area Estimation Details (m^2)	Total Estimated Area (m^2)
		Detected	3	57200, 272800, 1600	331600
		Detected	11	21200, 24500, 2800, 600, 400, 102300, 2300, 7800, 3900, 2700, 22500	191000
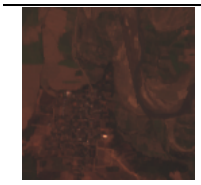		None	0	-	-
		Detected	10	8600, 8700, 600, 1900, 6700, 4300, 1200, 37500, 29600, 1400	100500

The object-level statistics reported in Table 1 are obtained through post-processing using Connected Component Labeling (CCL), which separates individual landslide objects from pixel-wise segmentation outputs. This process enables the transformation of dense segmentation maps into structured quantitative information, including the number of detected events and their corresponding area estimates.

Across the analyzed samples, images containing multiple small landslides as well as those dominated by fewer large events are consistently identified. For example, one sample contains three detected landslides with a combined estimated area of approximately 331,600 m^2, while another sample includes six landslide events covering approximately 61,500 m^2. These results confirm that the segmentation outputs preserve spatial coherence and scale variability in the detected landslide patterns.

Although minor deviations persist along complex slope boundaries and fragmented regions, the estimated spatial extents remain consistent with expected morphological characteristics. Overall, the analysis results indicate that the proposed framework produces stable object-level outputs that complement pixel-level segmentation performance and provide structured information suitable for post-landslide assessment.

4. DISCUSSIONS

This study demonstrates that integrating U-Net–based semantic segmentation with multi-source remote sensing data and cloud-oriented processing provides a reliable and operational framework for post-landslide mapping. Beyond performance metrics, the key finding lies in the consistent model behavior across training, validation, and testing phases, indicating that the proposed pipeline captures

Vol. 7, No. 2, April 2026, Page. 1040-1055
https://jutif.if.unsoed.ac.id
DOI: https://doi.org/10.52436/1.jutif.2026.7.2.5617

generalizable spatial characteristics of landslides rather than overfitting to localized features, a limitation frequently reported in previous studies.

The recall-oriented prediction behavior represents an appropriate trade-off for post-disaster applications, where missing landslide occurrences poses a greater risk than moderate overestimation of affected areas. Prior research highlights the importance of prioritizing recall in disaster-related mapping to reduce false negatives [26], [28]. The balanced precision–recall relationship achieved in this study further confirms its suitability for operational post-disaster deployment.

In comparison with existing U-Net–based landslide segmentation studies, the obtained F1-score and IoU demonstrate competitive and stable performance. While several studies report similar accuracy, they often rely on single-source imagery or geographically limited datasets, constraining generalization [1], [29]. The integration of spectral features (RGB and NDVI) with terrain-derived information (slope and elevation) improves robustness across diverse geomorphological conditions, supporting findings that multi-source data fusion enhances deep learning–based landslide detection [9].

Spatial inaccuracies along complex slope boundaries remain a persistent challenge due to gradual terrain transitions and ambiguous boundary definitions in high-resolution remote sensing data [30], [31]. Nevertheless, the strong correspondence between predicted and reference masks across most regions indicates that the model effectively captures dominant landslide morphology.

A notable contribution of this work is the extension from pixel-level segmentation to object-level analysis using Connected Component Labeling. Unlike prior studies that emphasize pixel-based metrics or qualitative visualization [29], [32], this approach enables quantitative estimation of landslide event counts and affected areas, providing actionable indicators for post-disaster assessment and intervention prioritization [22], [30].

From an Informatics and Computer Science perspective, the results underscore the role of cloud-based deployment in operationalizing deep learning for large-scale disaster mapping. The demonstrated feasibility of scalable, cloud-integrated segmentation pipelines supports recent calls for systems that combine deep learning and cloud computing to enable parallel processing, scalable inference, and real-world usability [33], [34].

Overall, this study shows that U-Net–based segmentation, when integrated with multi-source data, structured post-processing, and cloud infrastructure, can evolve from a methodological approach into a scalable, system-oriented solution for post-landslide disaster mitigation.

5. CONCLUSION

This study demonstrates that a cloud computing–based U-Net framework integrated with multi-source remote sensing data provides a reliable and operational solution for post-landslide satellite image segmentation. Consistent performance across training, validation, and testing phases indicates that the proposed pipeline demonstrates improved robustness across heterogeneous terrain conditions of landslides rather than overfitting to localized patterns. The recall-oriented prediction behavior further aligns with post-disaster requirements, where minimizing missed detections is critical for effective emergency response.

Rather than proposing a new network architecture, the principal contribution lies in operationalizing deep learning through multi-source data integration, object-level post-processing, and scalable cloud-based deployment. Extending pixel-level segmentation to object-level analysis enables the estimation of landslide event counts and affected areas, delivering actionable information for disaster assessment and prioritization. Although the framework remains dependent on annotated data and exhibits boundary uncertainty in complex terrain, it advances post-disaster mapping from a purely experimental segmentation task toward a scalable, cloud-enabled, and decision-oriented computational system for real-world disaster risk management.

Vol. 7, No. 2, April 2026, Page. 1040-1055
https://jutif.if.unsoed.ac.id
DOI: https://doi.org/10.52436/1.jutif.2026.7.2.5617

CONFLICT OF INTEREST

The authors declare that there is no conflict of interest between the authors or with research object in this paper.

REFERENCES

[1] D. Gómez, E. F. García, and E. Aristizábal, "Spatial and temporal landslide distributions using global and open landslide databases," *Nat. Hazards*, vol. 117, no. 1, pp. 25–55, 2023, doi: 10.1007/s11069-023-05848-8.

[2] N. Casagli, E. Intrieri, V. Tofani, G. Gigli, and F. Raspini, "Landslide detection, monitoring and prediction with remote-sensing techniques," *Nat. Rev. Earth Environ.*, vol. 4, no. 1, pp. 51–64, 2023, doi: 10.1038/s43017-022-00373-x.

[3] H. A. H. Al-Najjar, B. Pradhan, B. Kalantar, M. I. Sameen, M. Santosh, and A. Alamri, "Landslide Susceptibility Modeling: An Integrated Novel Method Based on Machine Learning Feature Transformation," *Remote Sens.*, 2021, doi: 10.3390/rs13163281.

[4] J. Li, J. Qin, K. I. Kang, M. Liang, K. Liu, and X. Ding, "Enhanced Spatiotemporal Landslide Displacement Prediction Using Dynamic Graph-Optimized GNSS Monitoring," *Sensors*, 2025, doi: 10.3390/s25154754.

[5] N. Zhou, J. Hong, W. Cui, S. Wu, and Z. Zhang, "A Multiscale Attention Segment Network-Based Semantic Segmentation Model for Landslide Remote Sensing Images," *Remote Sens.*, 2024, doi: 10.3390/rs16101712.

[6] A. Alfian, H. Jibran, I. Irmawati, M. F. I. Massinai, and H. Hasanuddin, "Pemanfaatan Penginderaan Jauh Dalam Mitigasi Bencana Longsor Daerah Kabupaten Sukabumi, Jawa Barat, Indonesia," *J. Tek. SILITEK*, vol. 2, no. 01, pp. 47–55, 2022, doi: 10.51135/jts.v2i01.48.

[7] B. Yanuargi and E. Utami, "Inception-ResNet-V2 The U-Net Encoder for Road Segmentation using Sentinel 2A," *ComTech Comput. Math. Eng. Appl.*, vol. 16, no. December, pp. 127–138, 2025, doi: 10.21512/comtech.v16i2.12089.

[8] M. A. Lasaiba, "Sistem Informasi Geografi dan Penginderaan Jauh dalam Pemetaan Zona Longsor Lahan di Kawasan Terbangun," *STRING (Satuan Tulisan Ris. dan Inov. Teknol.*, vol. 7, no. 3, p. 344, 2023, doi: 10.30998/string.v7i3.16161.

[9] C. Fang, X. Fan, H. Zhong, L. Lombardo, H. Tanyas, and X. Wang, "A Novel Historical Landslide Detection Approach Based on LiDAR and Lightweight Attention U-Net," 2022. doi: 10.3390/rs14174357.

[10] N. Siddique, S. Paheding, C. P. Elkin, and V. Devabhaktuni, "U-Net and Its Variants for Medical Image Segmentation: A Review of Theory and Applications," *IEEE Access*, vol. 9, pp. 82031–82057, 2021, doi: 10.1109/ACCESS.2021.3086020.

[11] J. Hendrik *et al.*, "Multi-Class Brain Tumor Segmentation and Classification in MRI Using a U-Net and Machine Learning Model," *J. Tek. Inform.*, vol. 6, no. 5 SE-Articles, pp. 3844–3856, Oct. 2025, doi: 10.52436/1.jutif.2025.6.5.5369.

[12] E. T. Rompisa and G. P. Kusuma, "Brain Tumor Segmentation From MRI Images Using MLU-Net with Residual Connections," *J. Tek. Inform.*, vol. 6, no. 5 SE-Articles, pp. 3445–3455, Oct. 2025, doi: 10.52436/1.jutif.2025.6.5.4742.

[13] F. Faturrohman, O. Nurdiawan, W. Prihartono, and R. Herdiana, "Enhanced U-Net Cnn For Multi-Class Segmentation And Classification Of Rice Leaf Diseases In Indonesian Rice Fields," *J. Tek. Inform.*, vol. 6, no. 5 SE-Articles, pp. 3124–3135, Oct. 2025, doi: 10.52436/1.jutif.2025.6.5.5258.

[14] S. R. Meena *et al.*, "Landslide Detection in the Himalayas Using Machine Learning Algorithms and U-Net," *Landslides*, vol. 19, no. 5, pp. 1209–1229, 2022, doi: 10.1007/s10346-022-01861-3.

[15] W. Xu *et al.*, "Combining Numerical Simulation and Deep Learning for Landslide Displacement Prediction: An Attempt to Expand the Deep Learning Dataset," *Sustainability*, 2022, doi: 10.3390/su14116908.

[16] S. M. Hussaine, L. Mu, Y. Lu, and S. S. Hussain, "Landslide Image Segmentation with Attention Residual U-Net: A Hybrid Deep Learning Model," *Procedia Comput. Sci.*, vol. 258, pp. 2029–

Vol. 7, No. 2, April 2026, Page. 1040-1055
https://jutif.if.unsoed.ac.id
DOI: https://doi.org/10.52436/1.jutif.2026.7.2.5617

2039, 2025, doi: 10.1016/j.procs.2025.04.453.
[17] Z. Dong, S. An, J. Zhang, J. Yu, J. Li, and D. Xu, "L-Unet: A Landslide Extraction Model Using Multi-Scale Feature Fusion and Attention Mechanism," *Remote Sens.*, vol. 14, no. 11, p. 2552, 2022, doi: 10.3390/rs14112552.
[18] M. Tang, Y. He, M. Aslam, E. Akpokodje, and S. F. Jilani, "Enhanced U-Net++ for Improved Semantic Segmentation in Landslide Detection," 2025. doi: 10.3390/s25092670.
[19] Z. Hu *et al.*, "Comparative Evaluation of State-of-the-Art Semantic Segmentation Networks for Long-Term Landslide Map Production," *Sensors*, vol. 23, no. 22, p. 9041, 2023, doi: 10.3390/s23229041.
[20] J. Vega and C. Hidalgo, "Evaluation of U-Net transfer learning model for semantic segmentation of landslides in the Colombian tropical mountain region," *MATEC Web Conf.*, vol. 396, 2024, [Online]. Available: https://doi.org/10.1051/matecconf/202439619002
[21] S. Gupta, S. Modgil, A. Kumar, U. Sivarajah, and Z. Irani, "Artificial intelligence and cloud-based Collaborative Platforms for Managing Disaster, extreme weather and emergency operations," *Int. J. Prod. Econ.*, vol. 254, p. 108642, 2022, doi: https://doi.org/10.1016/j.ijpe.2022.108642.
[22] X. Ren, X. Wu, D. Zhai, X. Wang, N. He, and M. Tarif, "ResM-FusionNet for efficient landslide detection algorithm with a hybrid architecture," *Sci. Rep.*, vol. 15, no. 1, p. 13080, 2025, doi: 10.1038/s41598-025-98230-6.
[23] G. Y. Kim, "Adam Optimization with Adaptive Batch Selection," in *The Thirteenth International Conference on Learning Representations*, 2025. doi: https://doi.org/10.48550/arXiv.2512.06795.
[24] H. Sun, S. Yang, R. Wang, and K. Yang, "Study on a Landslide Segmentation Algorithm Based on Improved High-Resolution Networks," 2024. doi: 10.3390/app14156459.
[25] J. Li, Q. LI, K. ZHENG, J. Lu, L. WEI, and Q. XIANG, "MF-L-UNet++: A Multi-scale Feature Recognition Algorithm for Landslide Images," *IEICE Trans. Inf. Syst.*, vol. E108.D, pp. 1058–1071, Sep. 2025, doi: 10.1587/transinf.2024EDP7280.
[26] O. Ghorbanzadeh, A. Crivellari, P. Ghamisi, H. Shahabi, and T. Blaschke, "A comprehensive transferability evaluation of U-Net and ResU-Net for landslide detection from Sentinel-2 data (case study areas from Taiwan, China, and Japan)," *Sci. Rep.*, vol. 11, no. 1, p. 14629, 2021, doi: 10.1038/s41598-021-94190-9.
[27] S. Ji, D. Yu, C. Shen, W. Li, and Q. Xu, "Landslide detection from an open satellite imagery and digital elevation model dataset using attention boosted convolutional neural networks," *Landslides*, vol. 17, no. 6, pp. 1337–1352, 2020, doi: 10.1007/s10346-020-01353-2.
[28] S. Bachri, K. Sastro Bangun Utomo, S. Sumarmi, M. Naufal Fathoni, and Y. Eka Aldianto, "Optimalisasi Model Artificial Neural Network Menggunakan Certainty Factor (C-ANN) Untuk Pemetaan Kerawanan Tanah Longsor Skala Semi-Detil di DAS Bendo, Kabupaten Banyuwangi," *Maj. Geogr. Indones.*, vol. 35, no. 1, p. 1, 2021, doi: 10.22146/mgi.57869.
[29] C. Cao *et al.*, "Comparative Study on Potential Landslide Identification with ALOS-2 and Sentinel-1A Data in Heavy Forest Reach, Upstream of the Jinsha River," 2022. doi: 10.3390/rs14091962.
[30] X. Shao, Y. Qiang, J. Li, L. Li, X. Zhao, and Q. Wang, "Semantic Segmentation of Remote Sensing Image Based on Contextual U-Net," p. 59, 2023, doi: 10.1117/12.2692004.
[31] F. Shaar, A. Yılmaz, A. E. Topcu, and Y. I. Alzoubi, "Remote Sensing Image Segmentation for Aircraft Recognition Using U-Net as Deep Learning Architecture," *Appl. Sci.*, vol. 14, no. 6, p. 2639, 2024, doi: 10.3390/app14062639.
[32] A. Abedalla, M. Abdullah, M. Al-Ayyoub, and E. Benkhelifa, "Chest X-ray pneumothorax segmentation using U-Net with EfficientNet and ResNet architectures," *PeerJ Comput. Sci.*, vol. 7, p. e607, 2021, doi: 10.7717/peerj-cs.607.
[33] C. Gupta, I. Johri, K. Srinivasan, Y. Hu, S. M. Qaisar, and K.-Y. Huang, "A Systematic Review on Machine Learning and Deep Learning Models for Electronic Information Security in Mobile Networks," *Sensors*, 2022, doi: 10.3390/s22052017.
[34] A. Vandoit, B. Blanco, L. Turon, and C. Killisly, "Cloud Detection on Satellite Imagery Using U-Net Architecture," p. 4, 2023, doi: 10.1117/12.2683412.